Iran J Ped Hematol Oncol. 2026, Vol. 16, No. 4, 1031-1051

Original Article

Feasibility and Dosimetric Evaluation of Beta-Emitting Sources in Surface Mold Brachytherapy for Oral Rhabdomyosarcoma: A Monte Carlo Study

Shahriyar Seraj[1] MSc, Shiva Rahbar Yazdi[2] PhD, Soroush Najafi Sarvestani[1] MSc, Mohammad Hosein Zare[*1] PhD, Saeedeh Hajihosseini[3] PhD

[1] Department of Medical Physics, School of Medicine, Shahid Sadoughi University of Medical Sciences, Yazd, Iran
[2] Department of Medical Physics, School of Medicine, Tehran University of Medical Sciences, Tehran, Iran
[3] Assistant Professor, Medical Nanotechnology and Tissue Engineering Research Science Institute, Shahid Sadoughi University of Medical Sciences, Yazd, Iran

*Corresponding Author: Dr. Mohammad Hosein Zare, Associate Professor, Department of Medical Physics, School of Medicine, Shahid Sadoughi University of Medical Sciences, Yazd, Iran. Email: mhzare2009@Gmail.Com. ORCID ID: 0000-0002-7823-1146.

Received: May 6, 2026
Accepted: July 12, 2026

Abstract

Background: This study aimed to evaluate the feasibility and dosimetric characteristics of $^{90}Sr/^{90}Y$ and ^{188}Re sources for treating superficial oral rhabdomyosarcoma (RMS) using a surface mold brachytherapy approach.

Materials and Methods: In this Monte Carlo simulation study, TG-149 dosimetric parameters were calculated to validate the source models. A patient-specific surface mold was then simulated for a 2.0-cm superficial tongue RMS lesion in a 5-year-old child anatomical model based on International Commission on Radiological Protection Publication 156. The effects of radionuclide type, number of active sources per catheter, catheter arrangement, and total number of catheters on dose rate, treatment time, and dosimetric characteristics were evaluated. Also, cylindrical ^{188}Re plaques with a 3.0-cm diameter and thicknesses of 0.1 and 0.2 cm were investigated.

Results: Reference dose rates were 0.54 ± 0.00 $Gy.min^{-1}.mCi^{-1}$ for $^{90}Sr/^{90}Y$ and 7.24 ± 0.01 $cGy.\mu Ci^{-1}.h^{-1}$ for ^{188}Re. In the catheter-based design, increasing the number of loaded sources increased dose rate and reduced the flatness (*F*), while central catheter placement provided the highest dose rate together with lower symmetry (*S*) and penumbra (*P*). Increasing the number of catheters from 3 to 20 reduced the treatment time from 2307.4 to 413.7 min for $^{90}Sr/^{90}Y$ and from 268.5 to 52.4 min for ^{188}Re. For $^{90}Sr/^{90}Y$, *F* ranged from 16.0% to 19.5%, *S* reached 1.06, and *P* reached 1.09 cm; corresponding values for ^{188}Re were 15.4%-18.3%, 1.10, and 1.13 cm, respectively. The 0.2-cm-thick ^{188}Re plaque achieved a dose rate of 433.4 $cGy.min^{-1}$ and reduced treatment time to less than 1 min, but showed *F* = 22.3% and *S* = 1.36.

Conclusion: Catheter- and plaque-based beta-emitting brachytherapy geometries showed limitations for treating superficial oral RMS at a 0.5-cm prescription depth. These limitations were primarily related to restricted beta-particle penetration and nonuniform lateral dose distribution.

Keywords: Beta Particles; Brachytherapy; Monte Carlo Method; Rhabdomyosarcoma

[DOI: 10.18502/ijpho.v16i4.22759]

Introduction

Among pediatric malignancies, rhabdomyosarcoma (RMS) remains the most common soft-tissue sarcoma, with current evidence suggesting that it originates from primitive skeletal muscle progenitor cells (1, 2). Although RMS can arise in almost any anatomical site, approximately 35% of cases occur in the head and neck area, where clinical presentation is often highly variable (3). Local therapeutic approaches such as surgery and radiotherapy (RT), can be challenging in early childhood and at anatomically sensitive sites because of the risk of long-term treatment-related complications (4). Furthermore, RT is associated with additional concerns, including radiation-induced mandibular injury and the potential development of secondary malignancies (5).

Given the susceptibility of critical adjacent structures, such as the salivary glands, mandible, and eyes to radiation-induced damage during external beam radiation therapy (EBRT), brachytherapy (BT) has emerged as an important modality (6, 7). According to the GEC-ESTRO recommendations, exclusive BT can achieve local control rates exceeding 90% for T_1-T_2N_0 tumors, whereas combined approaches involving EBRT followed by a BT boost have also been reported for selected cases (8). BT delivers radiation by positioning sealed radioactive sources in close proximity to or within the tumor, thereby enabling highly localized dose deposition (9). High-dose-rate (HDR) BT offers several advantages, including precise dose conformity, steep dose fall-off that limits irradiation to surrounding normal tissues, and reduced overall treatment time duration hypofractionated regimens (10).

Surface mold brachytherapy (SMB) using HDR sources has demonstrated low toxicity to adjacent critical structures in the management of oral tumors, including RMS (11). HDR SMB is a suitable treatment option for selected superficial head and neck tumors, including intra-oral lesions, particularly when the target can be adequately encompassed by the prescribed BT depth (12). In this technique, a patient-specific mold is fabricated according to the size and geometry of the tumor, and catheters containing the radioactive source are positioned within the mold to maintain close proximity to the tumor surface. This approach facilitates adequate target dose coverage while minimizing radiation exposure to the surrounding normal tissues (13).

Previous studies have extensively investigated gamma-emitting sources such as ^{192}Ir, ^{125}I, and ^{198}Au, for the treatment of oral cavity cancers using SMB (11, 14, 15). More recently, beta-emitting sources have been investigated for the treatment of superficial malignancies in organs such as the skin (16) and the eye (17). Beta radiation offers several favorable characteristics, including rapid energy deposition within the first few millimeters of tissue, and an effective penetration depth generally reported to be less than 1.0 cm (18). These characteristics may enable effective treatment of superficial tumors while limiting irradiation of surrounding healthy tissues.

Because beta-emitting sources exhibit a steep dose fall-off over short distances, accurate characterization of their dose distributions requires precise dosimetric and computational methods (19). Monte Carlo (MC) simulations are particularly useful for this purpose because they enable detailed characterization of dose distributions under different treatment conditions. This approach offers several advantages, including the ability to evaluate dose at arbitrary positions and angles, high reproducibility, assessment of different treatment scenarios, and reduced dependence on physical detector positioning (20).

To the best of our knowledge, the potential application of beta-emitting sources for intraoral BT using an SMB approach remains largely unexplored. Therefore, this study aimed to evaluate the dosimetric performance and feasibility of ^{90}Sr/^{90}Y and ^{188}Re sources for superficial oral RMS using MC simulations. Specifically, the effects of source type, number of active sources per catheter, catheter arrangement, and total number of catheters on dose rate, treatment time, and dose distribution were investigated. In addition, an ^{188}Re radioactive plaque was evaluated as an alternative source geometry for superficial oral lesions.

[DOI: 10.18502/ijpho.v16i4.22759]

Material and Methods

Characterization and simulation validations of the $^{90}Sr/^{90}Y$ and ^{188}Re sources

In this study, two clinically relevant beta-emitting sources, $^{90}Sr/^{90}Y$ and ^{188}Re, were selected for evaluation because of their potential applicability to the treatment of superficial oral cancers. Detailed elemental composition and material densities for both sources are summarized in Table I.

The $^{90}Sr/^{90}Y$ source was modeled according to the 5F design of the Novoste Beta-Cath system. The source consists of a cylindrical ceramic core composed of SiO_2, and uniformly loaded with $^{90}Sr/^{90}Y$. The ceramic core has a diameter of 0.56 mm and a length of 2.50 mm and is encapsulated within an SS304 stainless-steel capsule with a thickness of 0.04 mm along the lateral surface and 0.05 mm at both ends. The geometric parameters were based on previously reported specifications of the Novoste Beta-Cath 5F source. Each $^{90}Sr/^{90}Y$ seed was assigned a nominal activity of 5 mCi (185 MBq) consistent with the reported activity of the Novoste Beta-Cath source (21). The activity was assumed to be uniformly distributed throughout the active core. For a configuration containing N loaded seeds, the total implanted activity was calculated as $N \times$ 5 mCi. The $^{90}Sr/^{90}Y$ decay chain produces continuous beta spectra, with maximum beta-particle energies of approximately 0.546 MeV for ^{90}Sr and 2.28 MeV for ^{90}Y. The beta-emission spectra used in the present study were obtained from International Commission on Radiological Protection (ICRP) Publication 107 (22).

The ^{188}Re source geometry was adopted from the design reported by Khorshidi *et al.* (23). The seed was produced using a sol-gel derived bioactive glass matrix shaped into a cylindrical with a diameter of 0.30 mm and a length of 1.60 mm. The final seed consisted of a homogeneous mixture of rhenium, silicon, and calcium, with the material composition and density provided in Table I. This radionuclide emits beta particles with a maximum energy of 2.12 MeV, together with a low-intensity gamma component at 155 keV. According to Khorshidi *et al.* (23), the specific activity of the produced ^{188}Re was 3 $GBq.mg^{-1}$ after 18 h of neutron irradiation of 2 mg of $^{187}ReO_2$. In the present study, this specific activity was used as the basis for assigning the activity of the modeled ^{188}Re seed. The activity of each seed was calculated from the ^{188}Re mass contained in the modeled seed and the reported specific activity of 3 $GBq.mg^{-1}$.

For both radionuclides, all loaded seeds within a given catheter configuration were assumed to have identical activity and to be positioned according to the source-loading arrangements described in the treatment-plan simulations. No activity decay during an individual irradiation session was considered because the treatment duration was short relative to the half-life of $^{90}Sr/^{90}Y$. For ^{188}Re, the activity corresponding to the reported production condition was used for the treatment time calculations, and radioactive decay during irradiation was neglected. These activities and loading assumptions were applied consistently to the catheter-based and plaque-based configurations to ensure reproducibility of the simulated dose rates and treatment times.

To validate the source simulations, the intravascular BT dose-calculation formalism was applied. The dosimetric parameters, including the reference dose rate and the radial dose function, were determined according to the recommendations of the American Association of Physicists in Medicine (AAPM) Task Group 149 (TG-149) (24). TG-149 recommends the use of the TG-43 formalism in spherical coordinates, with the reference absorbed dose rate in water specified at a radial distance of 0.2 cm from the source center rather than air-kerma strength. This modification is necessary because air-kerma strength is not an appropriate source-strength specification for beta-emitting sources. A line-source approximation was employed to compute the geometric function required for these dosimetric calculations.

Treatment planning

For oral tumors classified as T_1-T_2N_0 and measuring less than 4.0 cm in diameter, BT alone has been reported as an effective treatment modality (6, 25). In the present study, a spherical tumor with a diameter of 2.0 cm was assumed to be located within the superficial layer of the tongue. The design of the surface mold was based on

[DOI: 10.18502/ijpho.v16i4.22759]

configurations reported in previous clinical studies (8, 12, 25, 26). Polymethyl methacrylate (PMMA) was selected as the mold material. The mold was designed with a diameter of 3.0 cm and a thickness of 0.5 cm, providing sufficient thickness for attenuation of the beta radiation. In accordance with previously published oral BT protocols (8, 27), a dose of 3 Gy per fraction was prescribed at a depth of 0.5 cm beneath the mold surface. All anatomical and tissue-composition data, including the density and elemental compositions of the simulated tongue tissue, were obtained from the ICRP Publication 156 and corresponded to a 5-year-old child.

The simulation parameters included the type of beta-emitting radionuclide (^{90}Sr/^{90}Y or ^{188}Re), the number of active sources per catheter, catheter placement geometry, and the total number of source-loaded catheters. The inter-catheter spacing for each configuration was determined geometrically based on the mold diameter and catheter diameter to achieve peripheral placement, uniform spacing, or central clustering. The spacing between adjacent catheters was calculated from the mold diameter (D_{mold}), the number of catheters ($M_{catheter}$), and the catheter diameter ($D_{catheter}$). For each configuration, the two-dimensional (2D) dose distribution and dose rate at the prescription depth were calculated, and the corresponding treatment time was determined. In an additional scenario, the ^{188}Re source was modeled as a cylindrical radioactive plaque attached to the mold, with a diameter of 3.0 cm and two thicknesses (0.1 and 0.2 cm). For each plaque configuration, 2D dose distribution, the dose rate at the prescription depth, and irradiation time required to deliver the prescribed dose were evaluated.

Beam profile characteristics were quantitatively evaluated according to the methodology described in IEC 60976 (28). The dose profiles at a depth of 0.5 cm were analyzed to determine the flatness (*F*), symmetry (*S*), and penumbra (*P*). *F* was calculated using the maximum and minimum dose values within the central flat region of the dose profile. This region was defined as the central 80% of the distance between the two positions where the dose decreased to 50% of the central-axis dose. *S* was determined by comparing dose values at pairs of equidistant points on opposite sides of the central-axis within the same region. *P* was defined as the lateral distance between the 80% and 20% dose levels of the central-axis dose on each profile. The mathematical expressions used for calculating *F* and *S* are presented in Equations (1) and (2), while *P* was evaluated independently for each configuration from the corresponding dose profiles.

$$\%F = \frac{(D\max - D\min)}{(D\max + D\min)} \times 100$$

$$S = \max\left[\frac{D(y)}{D(-y)}\right]$$

MC simulation

The MCNPX code (version 2.6.0) was used to calculate absorbed doses and evaluate the resulting dose distributions. MCNPX is a general-purpose MC particle-transport code capable of modeling the interactions of various particles, including neutrons, photons, and electrons, across complex geometries. In this study, the MCPLIB04 cross-section library was employed for photon and electron transport simulations.

To validate the source simulations and calculate the dosimetric parameters according to the TG-149 recommendations, a spherical water phantom with a diameter of 30 cm was modeled. The cylindrical source was positioned at the center of the phantom, with its longitudinal axis aligned with the *Z*-axis. Toroidal cells were defined to calculate the absorbed dose at the distances specified by standard reference protocols (23, 29), and the *F8 tally was used to determine the energy deposition within these cells. An energy cut-off of 10 keV was applied to both photons and electrons throughout MC simulations.

Subsequently, a digital phantom of the human tongue was constructed, and the surface mold containing the radioactive source catheters was positioned on the tongue surface. Material compositions and densities were obtained from established reference databases, including the NIST XCOM database (30) and ICRP Publication

[DOI: 10.18502/ijpho.v16i4.22759]

156 (31). To determine the absorbed dose distribution within the tongue, a type-1 mesh tally with the "pedep" (particle energy deposition) option was employed. The rectangular mesh resolution was set at 1.0 × 1.0 × 0.1 mm^3. The mesh-tally output files were converted to text format using the "gridconv" software, after which MATLAB (R2017a) was used to reshape the data and generate the dose distributions. Finally, all dose values were normalized to the central-axis dose at the prescription depth, and isodose contours were generated at 300%, 200%, 150%, 100%, 80%, 50%, 30%, and 10% of the prescription dose.

Uncertainly analysis

The reliability of the MC simulations was evaluated by considering both statistical (Type A) and systematic (Type B) components, following the recommendations of TG-138 protocols (32). Type-A uncertainty was estimated from the relative standard deviation of the MC dose scores and reported as the statistical uncertainty of the calculated dose. The simulations were performed using 1-5 × 10^8 particle histories. During the validation stage, the mean statistical uncertainties in the reference dose rate were 0.19% for $^{90}Sr/^{90}Y$ and 0.08% for the ^{188}Re source. The corresponding mean statistical uncertainties in the radial dose function were 0.26% and 0.23%, respectively. For the clinical configurations, the mean statistical uncertainties of the dose rate at the prescription depth were 2.17% and 1.46% for the catheter-based molds employing $^{90}Sr/^{90}Y$ and ^{188}Re sources, respectively, and 1.31% for the ^{188}Re plaque geometry. These values were considered acceptable for comparative MC dosimetry.

Potential Type-B uncertainties were associated with source geometry, emission spectra, tissue-composition and density, catheter or plaque positioning, voxel size, and transport cut-off energies. The source dimensions and compositions were obtained from published source models (21, 23, 29), and the corresponding uncertainties were assumed to be less than 0.5%. The uncertainty associated with the beta emission spectrum was assumed to be below 1.0%, as beta dose distributions are only minimally affected by small variations in the emission spectrum, unlike photon-based dose calculations (32). The contribution of tissue-composition was estimated by repeating selected simulations with a water-equivalent material replacing the tongue tissue, resulting in an uncertainty of 1.9% in the dose rate at the prescription depth.

The uncertainty associated with catheter or plaque positioning was evaluated by introducing positional displacements ranging from 0.1 to 0.5 cm, yielding an estimated uncertainty of 1.1%. The corresponding uncertainty due to voxel size was determined by reducing the voxel thickness in the depth direction from 0.2 mm to 0.1 mm, resulting in 0.6%. Likewise, decreasing the transport cut-off energy from 10 keV to 1 keV, produced an estimated uncertainty of 2.0%. These tests indicated that the calculated dose distributions were not substantially affected by the tested numerical parameters.

The overall uncertainty was estimated by combining the Type-A and Type-B uncertainty components in quadrature (Equation 3). A coverage factor of k = 1 was used, corresponding approximately to a 68% confidence interval. The resulting combined uncertainty was 4.3% for the principal dosimetric quantities. Because the Type-B components represent systematic effects common to all compared configurations, only the statistical (Type-A) uncertainties are reported together with the individual dosimetric results.

$$U_{\text{total}} = \sqrt{U_A^2 + U_B^2} \qquad (3)$$

Results

The reference dose rates for the $^{90}Sr/^{90}Y$ and ^{188}Re sources were assessed to be 0.54 ± 0.00 $Gy.min^{-1}.mCi^{-1}$ and 7.24 ± 0.01 $cGy.\mu Ci^{-1}.h^{-1}$, respectively, consistent with the recommended units in references (29) and (23). Additionally, the radial dose function values for both sources at distances from 0.6 to 8.0 cm, along with the corresponding reference values and their relative differences are presented in Table II. As expected, this function decreased with increasing radial distance, and its rate of change (slope) was steeper for the ^{188}Re source than for the $^{90}Sr/^{90}Y$ source.

[DOI: 10.18502/ijpho.v16i4.22759]

Table III presents the effect of the number of sources loaded per catheter on the central-axis dose rate at the prescription depth, and the corresponding treatment time. As shown, increasing the number of sources to its maximum feasible value resulted in a higher dose rate. In addition, *F* decreased, indicating improved dose uniformity, although this was accompanied by a broader *P*. This effect is further illustrated in Figure 1. As shown in Figure 1 (a), when fewer sources were used, the higher isodose lines were concentrated at shallower depths, whereas the lower isodose levels extended to greater depths. Under this configuration, the lateral dose spread was greater, resulting in increased irradiation of the surrounding healthy tissues. In contrast, as shown in Figure 1 (b) for situation 6, the irradiation became more localized. In this scenario, *F* was improved and the higher isodose levels extended to greater depths.

Another part of the study examined the effect of different catheter placement configurations (peripheral, uniform, and central) within the mold. The corresponding results are presented in Table IV and Figure 2. Among the three configurations, central catheter placement resulted in the highest dose rate at the reference depth. In this situation, *F* was poorer than that observed for the other configurations, whereas the *P* was more favorable. Furthermore, as shown in Figure 2, the low-isodose regions were more confined in this configuration, resulting in a reduction in the volume of surrounding healthy tissue exposed to radiation.

Based on these findings, which reveals that maximizing the number of loaded sources per catheter and positioning the catheters centrally within the mold could improve dosimetric performance, an additional analysis was performed to investigate the effect of the total number of catheters. Table V and VI present the dose rates, corresponding treatment times, and dosimetric characteristics (*F*, *S*, and *P*) for the two radionuclides, ^{90}Sr/^{90}Y and ^{188}Re, using 3 to 20 catheters. Increasing the number of catheters allowed a greater number of sources to be loaded, which consequently increased the total activity. For ^{90}Sr/^{90}Y, the treatment time decreased substantially from 2307.4 min 3 catheters to 413.7 min with 20 catheters. The *F* and *S* values over this range varied from 16.0% to 19.5% and from 1.03 to 1.06, respectively. The maximum *P* value was 1.09 cm, obtained with 10 catheters containing 106 sources.

The ^{188}Re source demonstrated a more favorable trend in terms of treatment time and activity. The maximum total activity reached 229.6 MBq, compared with 38.1 MBq for ^{90}Sr/^{90}Y. Treatment times decreased from 268.5 min with 3 catheters to 52.4 min with 20 catheters. The *F* values ranged from 15.4% to 18.3%, representing lower values than those obtained for ^{90}Sr/^{90}Y. In contrast, *S* increased to a maximum of 1.10, while *P* reached a maximum of 1.13 cm, indicating less favorable *S* and a broader *P* compared with ^{90}Sr/^{90}Y.

Figure 3 illustrates the effect of the number of source-containing catheters on the resulting dose distribution. For both radionuclides, the cases with the minimum (3) and maximum (20) numbers of catheter are presented. With only 3 catheters, the high isodose levels (300%) extended to a depth of 0.1 cm and exhibited considerable lateral spread. With 20 catheters, the 300% isodose line disappears for ^{90}Sr/^{90}Y and became considerably more confined for ^{188}Re. In all other respects, the overall shape of the isodose curves remained nearly unchanged.

In a separate simulation, the ^{188}Re emitter was modeled as a cylindrical radioactive plaque with thicknesses of 0.1 and 0.2 cm and a diameter of 3.0 cm, positioned directly over the tumor surface. Increasing the plaque thickness from 0.1 to 0.2 cm approximately doubled the total plaque activity from 4.98 to 9.96 TBq and increased the dose rate at the prescription depth from 221.4 ± 2.9 to 433.4 ± 5.6 cGy.min^{-1}. Consequently, the treatment time decreased from 1.35 to 0.69 min. However, the lateral dose-profile parameters showed limited dose uniformity, with *F* values of 22.6 ± 1.1% and 22.3 ± 1.0% and *S* values of 1.24 ± 0.03 and 1.36 ± 0.04 for the 0.1- and 0.2-cm-thick plaques, respectively. The corresponding *P* values were 0.97 ± 0.03 and 1.08 ± 0.03 cm. For the 0.2-cm-thick plaque, the relatively high *F* and *S* values indicated pronounced lateral dose non-uniformity despite the substantially higher dose rate and

[DOI: 10.18502/ijpho.v16i4.22759]

shorter treatment time. Figure 4 presented the resulting dose distribution profiles for the plaque sources. The dose distribution exhibited pronounced non-uniformity, with a lateral spread of approximately 1.0 cm for the 100% isodose line. Consequently, a tumor with a diameter of 2.0 cm would be encompassed only by the 30% isodose level, potentially compromising the accuracy of dose delivery.

Table I: Physical properties and elemental composition of materials used in the simulation setup

Material	Elemental composition	Density (g.cm^{-3})	Reference	Material
^{90}Sr/^{90}Y source	O: 53.26 %, Si: 46.74 %	4.00	(21, 29)	^{90}Sr/^{90}Y source
^{188}Re source	Re: 20.00%, Si: 50.00%, Ca: 30.00%	2.35	(23)	^{188}Re source
SST 304 capsule	Fe: 67.00 %, Cr: 19.50 %, Ni: 10.50 %, Mn: 2.00 %, Si: 0.75 %, N: 0.10 %, C: 0.07 %, P: 0.05 %, S: 0.03 %	8.02	(16)	SST 304 capsule
Poly Ethylene catheter	C: 85.63%, H: 14.37%	0.94	(30)	Poly Ethylene catheter
Polymethyl Methacrylate mold	C: 59.99%, O: 31.96%, H: 8.05%	1.19	(30)	Polymethyl Methacrylate mold
Tongue	O: 71.10 %, C: 14.20 %, H: 10.20 %, N: 3.40 %, K: 0.40 %, S: 0.30 %, P: 0.20 %, Na: 0.10 %, Cl: 0.10 %	1.03	(31)	Tongue
Air	N: 75.04 %, O: 23.61 %, Ar: 1.27 %, H: 0.07 %, C: 0.01 %	1.20×10-3	(30)	Air

[DOI: 10.18502/ijpho.v16i4.22759]

*Table II: Radial dose function values for $^{90}Sr/^{90}Y$ and ^{188}Re sources obtained from Monte Carlo simulations**

	$^{90}Sr/^{90}Y$ source			^{188}Re source		
	g (r)			g (r)		
r (mm)	Present study	Reference study (29)	Difference (%)	Present study	Reference study (23)	Difference (%)
0.6	1.121±0.014	1.117	0.35	1.245±0.006	1.211	2.80
1.0	1.099±0.006	1.099	0.00	1.198±0.002	1.187	0.92
1.5	1.062±0.003	1.065	0.28	1.111±0.001	1.099	1.09
2.0	1.000±0.002	1.000	0.00	1.000±0.001	1.000	0.00
2.5	0.906±0.001	0.911	0.54	0.875±0.000	0.880	0.56
3.0	0.809±0.001	0.806	0.37	0.743±0.000	0.746	0.40
3.5	0.707±0.000	0.692	2.16	0.613±0.000	0.617	0.64
4.0	0.598±0.000	0.576	3.81	0.489±0.000	0.493	0.81
4.5	0.491±0.000	0.464	5.81	0.377±0.000	0.380	0.78
5.0	0.389±0.000	0.363	7.16	0.277±0.000	0.276	0.36
5.5	0.296±0.000	0.274	8.02	0.195±0.000	0.196	0.51
6.0	0.214±0.000	0.199	7.53	0.129±0.000	0.133	3.00
6.5	0.146±0.000	0.138	5.79	0.080±0.000	0.083	3.61
7.0	0.093±0.000	0.090	3.33	0.046±0.000	0.046	0.00
7.5	0.055±0.000	0.056	1.78	0.024±0.000	0.024	0.00
8.0	0.030±0.000	0.032	6.25	0.012±0.000	0.012	0.00

***Values are compared with published reference data from Ref. (29) for the $^{90}Sr/^{90}Y$ source and Ref. (23) for the ^{188}Re source.**

[DOI: 10.18502/ijpho.v16i4.22759]

Table III: Effect of the number of active ^{188}Re sources per catheter on the dose rate at the prescription depth, treatment time, and lateral dose-profile parameters for a 7-catheter mold configuration

Source-loading scenario	Total number of sources	Total source activity (GBq)	Dose rate (cGy.min^{-1})	Treatment time (min)	Flatness (%)	Symmetry	Penumbra (cm)
1	69	53.4	1.35±0.02	222.1	20.0±1.0	1.06±0.02	1.03±0.02
2	76	59.8	1.45±0.02	206.5	19.6±1.0	1.06±0.02	1.05±0.02
3	83	66.1	1.53±0.02	196.1	18.6±1.1	1.04±0.02	1.10±0.02
4	90	71.7	1.57±0.02	191.3	18.5±1.1	1.05±0.02	1.10±0.03
5	97	77.3	1.55±0.02	193.8	18.6±1.1	1.05±0.02	1.12±0.02
6	104 (maximum)	82.9	1.69±0.02	177.1	18.3±1.1	1.05±0.02	1.09±0.03

*Table IV. Effect of catheter arrangement on the dose rate at the prescription depth, treatment time, and lateral dose-profile parameters for a 7 -catheter ^{188}Re mold configuration**

Catheter arrangement	Inter-catheter spacing (cm)	Dose rate (cGy.min^{-1})	Treatment time (min)	Flatness (%)	Symmetry	Penumbra (cm)
Peripheral placement	$2 \times \left(\frac{\text{Dmold} - (\text{Mcatheter} \times \text{Dcatheter})}{\text{Mcatheter}}\right)$	1.41±0.02	212.3	19.5±1.2	1.05±0.03	1.14±0.03
Uniform placement	$\frac{\text{Dmold} - (\text{Mcatheter} \times \text{Dcatheter})}{\text{Mcatheter}}$	1.69±0.02	177.1	18.3±1.1	1.05±0.02	1.09±0.03
Central placement	$\frac{\text{Dmold} - (\text{Mcatheter} \times \text{Dcatheter})}{2 \times \text{Mcatheter}}$	2.33±0.03	128.5	19.9±0.9	1.03±0.02	1.05±0.02

*** The total number of sources and total source activity were identical for all catheter arrangements**

[DOI: 10.18502/ijpho.v16i4.22759]

Table V. Effect of the number of catheters on the total number of sources, total source activity, dose rate at the prescription depth, treatment time, and lateral dose-profile parameters for the $^{90}Sr/^{90}Y$ mold configuration

Number of catheters	Total number of sources	Total source activity (GBq)	Dose rate (cGy.min^{-1})	Treatment time (min)	Flatness (%)	Symmetry	Penumbra (cm)
3	33	6.1	0.130±0.002	2307.4	16.0±1.1	1.04±0.03	0.86±0.02
4	42	7.8	0.176±0.003	1700.7	17.5±1.2	1.05±0.02	0.98±0.02
5	53	9.8	0.209±0.003	1435.5	16.7±1.1	1.04±0.02	1.01±0.03
6	64	11.8	0.264±0.004	1136.1	16.8±1.1	1.05±0.02	1.07±0.02
7	75	13.9	0.310±0.004	966.1	16.4±1.1	1.03±0.02	1.02±0.03
8	86	15.9	0.339±0.005	883.1	18.2±1.3	1.03±0.03	1.07±0.03
9	95	17.6	0.382±0.006	784.2	18.8±1.1	1.04±0.02	0.99±0.03
10	106	19.6	0.431±0.006	695.3	19.5±1.1	1.05±0.02	1.09±0.03
11	117	21.6	0.475±0.007	632.0	18.7±1.1	1.04±0.02	1.02±0.03
12	128	23.7	0.515±0.008	582.2	17.3±1.1	1.04±0.02	1.00±0.03
13	139	25.7	0.558±0.008	537.1	18.4±1.1	1.04±0.04	0.98±0.03
14	148	27.4	0.602±0.009	498.2	18.4±1.1	1.05±0.03	1.05±0.03
15	159	29.4	0.628±0.009	477.4	17.5±1.1	1.03±0.02	1.05±0.03
16	170	31.4	0.661±0.010	453.6	17.7±1.1	1.04±0.02	1.05±0.03
17	177	32.7	0.678±0.010	442.6	18.6±1.1	1.05±0.02	1.00±0.03
18	188	34.8	0.698±0.011	429.6	18.6±1.1	1.06±0.02	1.00±0.03
19	195	36.1	0.701±0.011	427.7	18.7±1.2	1.04±0.02	0.99±0.03
20	206	38.1	0.725±0.011	413.7	17.6±1.2	1.04±0.02	1.00±0.03

[DOI: 10.18502/ijpho.v16i4.22759]

Table VI. Effect of the number of catheters on the total number of sources, total source activity, dose rate at the prescription depth, treatment time, and lateral dose-profile parameters for the ^{188}Re mold configuration

Number of catheters	Total number of sources	Total source activity (GBq)	Dose rate (cGy.min^{-1})	Treatment time (min)	Flatness (%)	Symmetry	Penumbra (cm)
3	52	38.3	1.12±0.01	268.5	17.2±1.0	1.07±0.02	1.07±0.02
4	70	49.4	1.46±0.02	206.1	15.4±1.1	1.06±0.02	1.01±0.02
5	88	62.2	1.77±0.02	169.8	17.6±1.1	1.05±0.02	1.08±0.03
6	104	71.7	1.95±0.03	153.6	17.3±1.0	1.06±0.02	1.05±0.03
7	120	82.9	2.38±0.04	126.0	16.9±1.1	1.05±0.02	1.03±0.03
8	138	97.3	2.77±0.04	108.4	17.6±1.1	1.06±0.02	1.13±0.03
9	156	106.8	2.94±0.04	101.9	16.6±1.1	1.04±0.02	1.10±0.03
10	172	119.6	3.21±0.05	93.5	15.9±1.1	1.07±0.02	1.05±0.03
11	194	129.2	3.82±0.06	78.6	18.3±1.1	1.05±0.02	1.03±0.03
12	212	143.5	4.21±0.06	71.2	16.7±1.1	1.05±0.02	1.05±0.03
13	222	151.5	4.08±0.06	73.5	17.0±1.1	1.03±0.02	1.04±0.03
14	238	164.2	4.40±0.06	68.2	15.8±1.0	1.09±0.02	1.11±0.03
15	254	173.8	4.67±0.07	64.2	16.6±1.1	1.04±0.02	1.07±0.03
16	274	183.4	4.87±0.07	61.6	17.2±1.1	1.10±0.03	1.06±0.03
17	288	197.7	5.25±0.08	57.2	16.8±1.1	1.10±0.03	1.10±0.03
18	306	207.3	5.42±0.08	55.3	16.3±1.1	1.06±0.02	1.11±0.03
19	320	216.9	5.63±0.08	53.2	16.8±1.1	1.06±0.02	1.11±0.03
20	340	229.6	5.72±0.09	52.4	18.3±1.1	1.03±0.02	1.05±0.03

[DOI: 10.18502/ijpho.v16i4.22759]

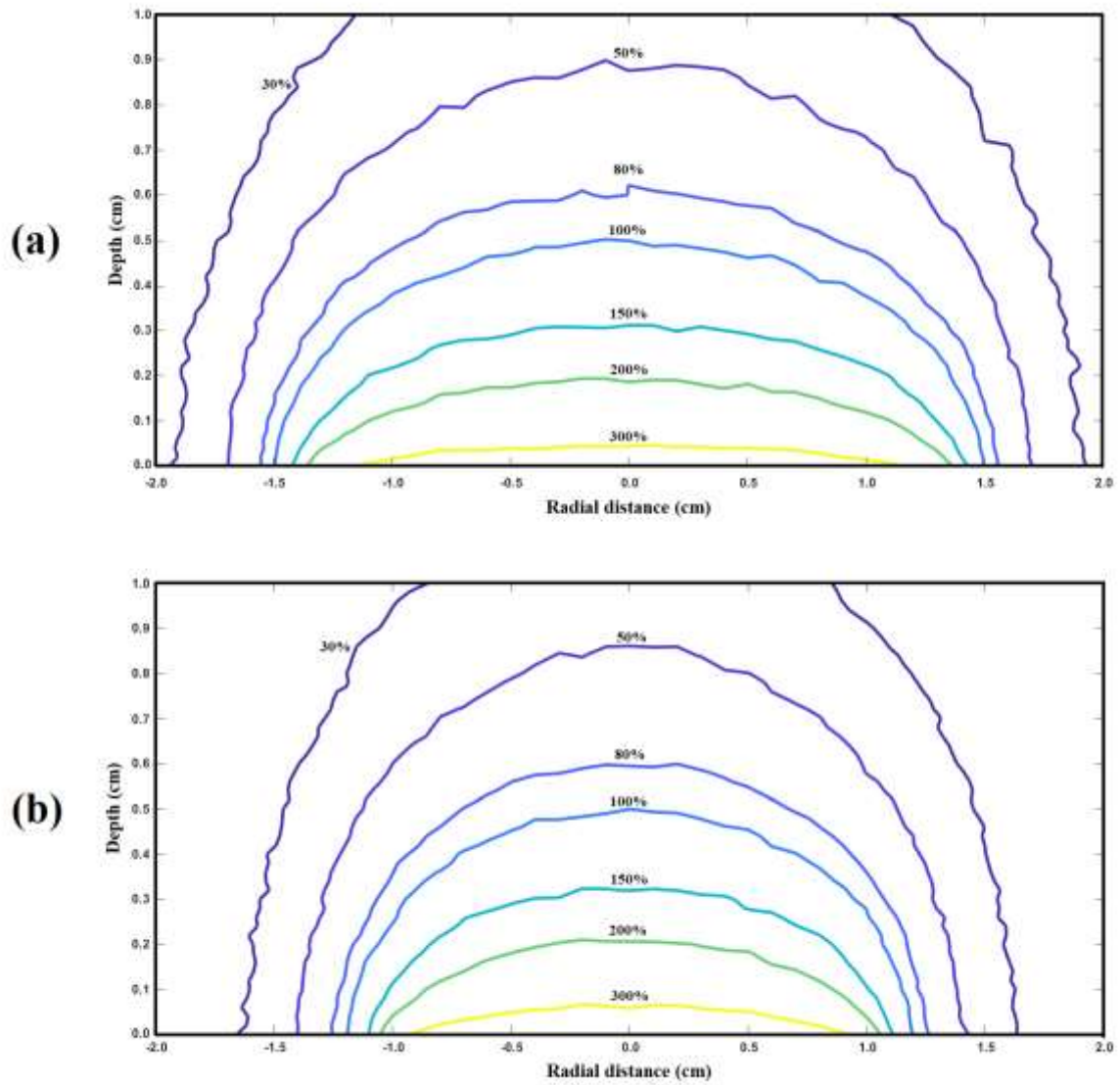

Figure 1. Dose distribution profiles along radial distance and depth for (a) situation 1 and (b) situation 6 of the ^{188}Re 7‑catheter mold, with situation 6 corresponding to the maximum number of active sources

[DOI: 10.18502/ijpho.v16i4.22759]

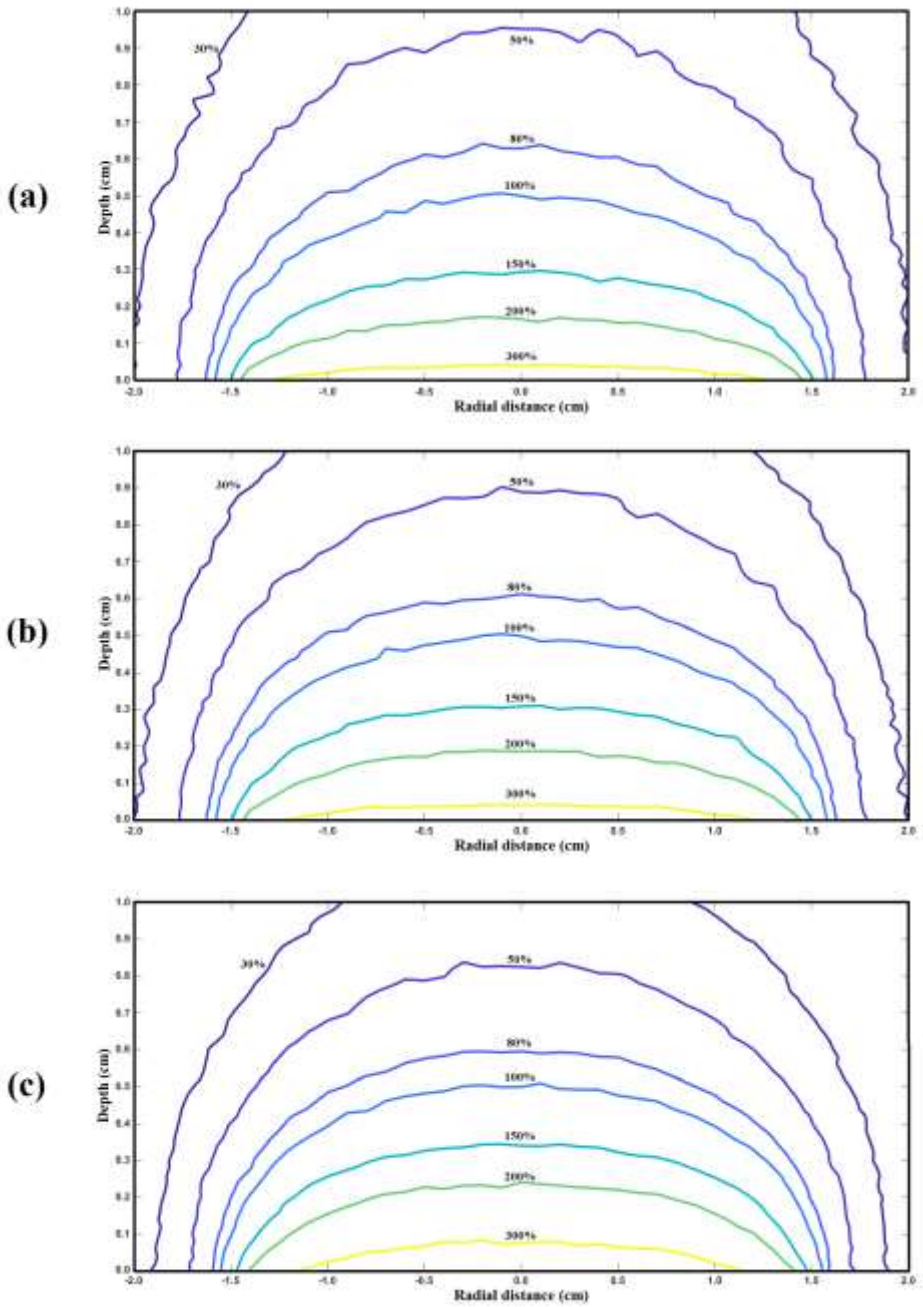

Figure 2. Dose distribution profiles along radial distance and depth for the ^{188}Re 7‑catheter mold with different catheter arrangements: (a) peripheral, (b) uniform, and (c) central

[DOI: 10.18502/ijpho.v16i4.22759]

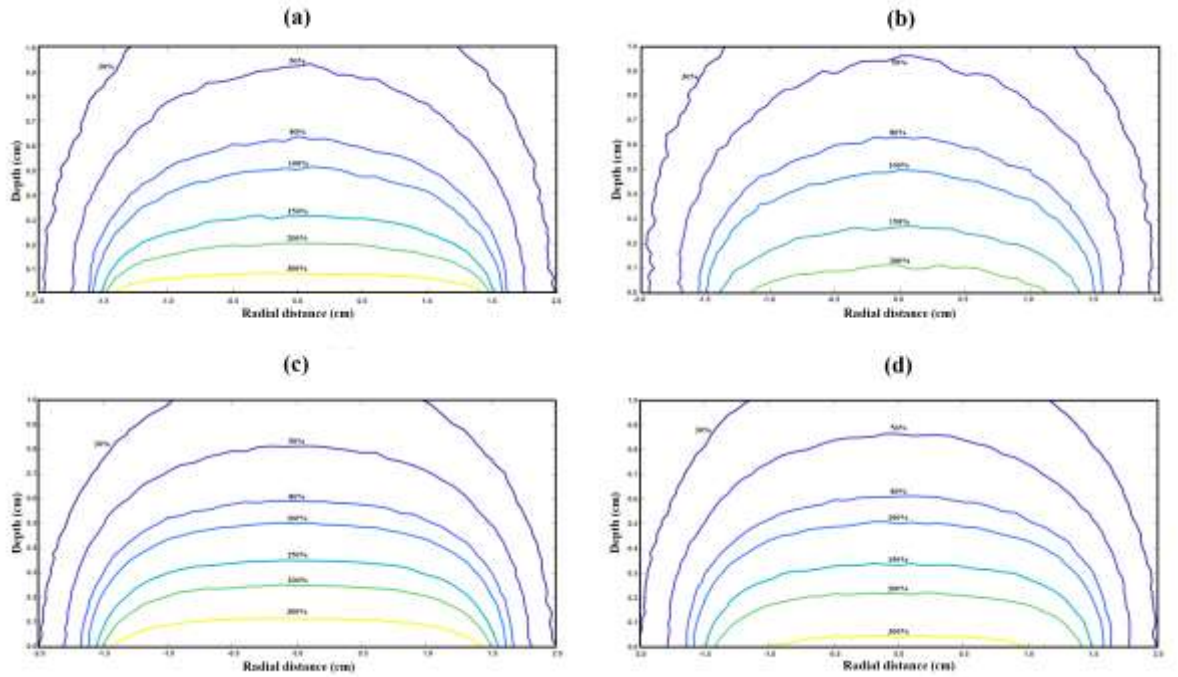

Figure 3: Dose distribution profiles along radial distance and depth for different catheter counts using $^{90}Sr/^{90}Y$ and ^{188}Re sources: (a) 3‑catheter and (b) 20‑catheter configurations for $^{90}Sr/^{90}Y$, and (c) 3‑catheter and (d) 20‑catheter configurations for ^{188}Re

[DOI: 10.18502/ijpho.v16i4.22759]

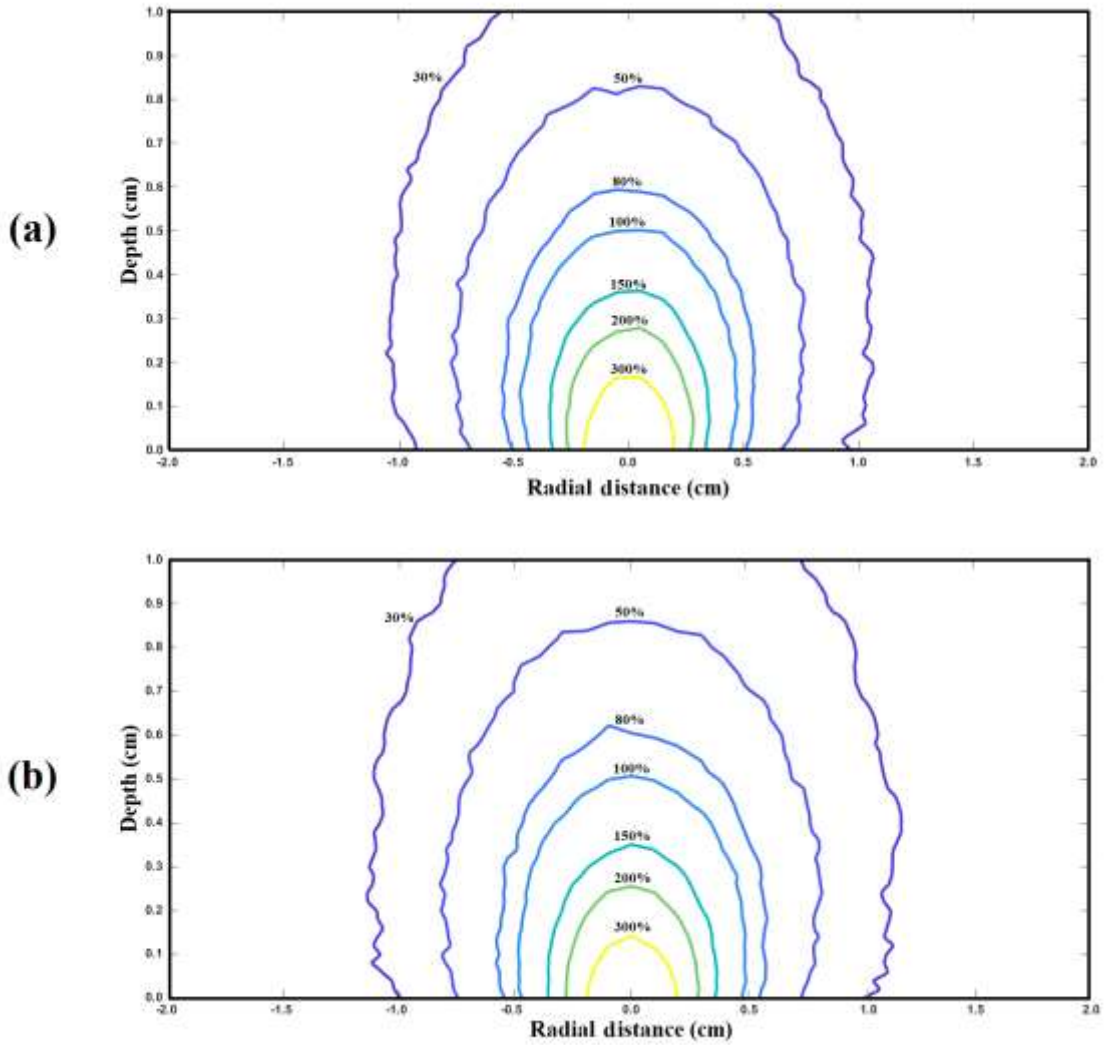

Figure 4: Dose distribution profiles along radial distance and depth for different thicknesses of the ^{188}Re radioactive plaque: (a) 0.1 cm and (b) 0.2 cm

Discussion

The present study demonstrated that the feasibility of using beta-emitting sources for intraoral SMB is strongly influenced by beta-particle penetration, source configuration, and treatment geometry. Although both ^{90}Sr/^{90}Y and ^{188}Re produced HDR near the mold surface, their limited penetration resulted in substantial dose attenuation with increasing depth. Consequently, achieving the prescribed dose at a depth of 0.5 cm required prolonged treatment times for catheter-based configurations, particularly with ^{90}Sr/^{90}Y. The alternative ^{188}Re plaque configuration substantially reduced the treatment time but resulted in inadequate dose uniformity and target coverage. These findings indicate that, under the conditions investigated, the principal limitation observed in this study was not the ability of beta-emitting sources to generate HDR near the mold surface. Rather, the main limitation was their ability to achieve adequate and sufficiently uniform dose coverage at clinically relevant depths.

The reliability of these findings is supported by the source-validation results. The reference dose rates calculated according to the TG-149 formalism showed close agreement with

[DOI: 10.18502/ijpho.v16i4.22759]

previously published data (23, 29). The reference dose rate obtained for the $^{90}Sr/^{90}Y$ source (0.54 ± 0.00 $Gy.min^{-1}.mCi^{-1}$) differed by less than 0.5% from the value reported by Wang and Li (32), whereas the rate calculated for ^{188}Re (7.24 ± 0.01 $cGy.\mu Ci^{-1}.h^{-1}$) showed a deviation of only 2.55% from that reported by Khorshidi et al. (23). The radial dose functions calculated for both isotopes also showed close agreement with the published data (Table II). For $^{90}Sr/^{90}Y$, discrepancies were below 1.0% at distances of up to 0.3 cm, with an overall mean deviation of 2.85%. For ^{188}Re, deviations were below 1.0% at most evaluated distances, with an overall mean deviation of 0.97%. This agreement supports the accuracy and robustness of the source models and provides confidence in the subsequent treatment-planning simulations.

The initial treatment-planning simulations focused on catheter-based placement of beta-emitting sources within the intraoral mold. Increasing the number of loaded catheters generally increased the dose rate and reduced the treatment time; however, the treatment duration remained clinically problematic, particularly for $^{90}Sr/^{90}Y$. Increasing the catheter number from 3 to 20 reduced the $^{90}Sr/^{90}Y$ treatment time from 2307.4 min to 413.7 min. Although this represents a substantial reduction, the resulting treatment time remains impractical for routine HDR treatment. The ^{188}Re source performed more favorably, with treatment times decreasing from 268.5 min with 3 catheters to 52.4 min with 20 catheters, reflecting its higher dose rate under the investigated conditions. Nevertheless, even the shortest catheter-based ^{188}Re treatment time may be lengthy compared with conventional HDR BT.

Despite the improvements obtained by increasing the number of catheters, the treatment times remained substantially longer than those typically associated with conventional HDR BT. These findings indicate that catheter-based beta BT, particularly with the investigated $^{90}Sr/^{90}Y$ activity, cannot provide clinically acceptable treatment times under the evaluated loading conditions. Possible strategies for reducing treatment time include increasing source activity within acceptable radiation-safety limits, increasing the number of active sources or catheters, optimizing catheter spacing and placement, and developing distributed or segmented higher-activity source arrays. However, increasing source strength or source number alone may adversely affect dose uniformity and normal-tissue exposure and would therefore require concurrent optimization of the applicator geometry and treatment plan.

The depth-dose characteristics of the beta sources provide an important explanation for the observed treatment limitations. Although the catheter-based approach produced reasonably uniform lateral dose distributions and limited dose deposition outside the treated region, the rapid dose fall-off of beta particles resulted in insufficient dose delivery at a lesion depth of 0.5 cm. Thus, the finding of good lateral dose uniformity does not necessarily imply adequate three-dimensional target coverage. This distinction is particularly important for superficial oral tumors, for which the target may extend several millimeters beneath the mucosal surface. In contrast, the greater penetration of conventional ^{192}Ir gamma radiation would be expected to provide better dose coverage at this depth, although at the expense of greater dose deposition beyond the target.

This difference is consistent with clinical experience with photon-based HDR BT for oral malignancies. HDR BT has been used successfully for selected early-stage oral cancers, with customized intraoral applicators containing one or more catheters providing conformal dose distributions and acceptable toxicity (25, 26). Several studies have also reported favorable outcomes using ^{192}Ir surface molds in pediatric and adult patients with oral or oropharyngeal RMS (1, 34, 35). For example, Takácsi-Nagy *et al.* (36) reported long-term outcomes in 45 patients with T_1-T_2N_0 tongue cancer treated with postoperative interstitial HDR BT using ^{192}Ir. The mean prescribed dose was 29 Gy, and the 5- and 10-year local control rates were both 85%, with grade 4 late soft-tissue necrosis occurring in 7% of patients. Although

[DOI: 10.18502/ijpho.v16i4.22759]

the interstitial technique differs from the surface mold configurations investigated in the present study, these clinical results provide a useful benchmark for the established efficacy and acceptable toxicity of conventional ^{192}Ir HDR BT.

According to the recommendations of the Indian BT Society (37), small superficial tumors of the facial skin and accessible mucosal lesions, including the oral cavity tumors, may be considered for ^{192}Ir HDR SMB. However, catheter loading, source dwell positions, and dwell times must be carefully optimized to limit irradiation of adjacent bone and cartilage. Compared with the rapid dose fall-off of beta-emitting sources, the greater penetration of ^{192}Ir gamma rays can improve dose coverage at clinically relevant depths, including the 0.5-cm prescription depth evaluated in the present study. This advantage is accompanied by increased dose deposition beyond the target, potentially increasing the risk of bone or cartilage necrosis if appropriate spacing, shielding, and treatment-plan optimization are not applied.

The use of beta-emitting sources in other clinical applications provides additional context for the present findings. Isotopes such as ^{90}Sr/^{90}Y and ^{188}Re have demonstrated favorable performance in the treatment of superficial skin malignancies because of their rapid dose fall-off and limited penetration (38-41). Similarly, beta-emitting plaques, including ^{106}Ru/^{106}Rh and ^{90}Sr/^{90}Y, have long been used for ocular tumors such as uveal melanoma and retinoblastoma (42). In these applications, limited penetration is advantageous because it allows high local doses to be delivered while reducing irradiation of deeper critical structures such as the optic nerve and lens. These established applications support the potential use of beta-emitting sources for other superficial targets; however, the present findings demonstrate that successful translation to intraoral tumors requires an applicator geometry specifically adapted to the target depth and shape.

To address the penetration and treatment-time limitations observed with catheter-based configurations, an alternative configuration consisting of a cylindrical ^{188}Re plaque placed directly on the tumor surface was evaluated. The 0.2-cm-thick plaque increased the dose rate at the prescription depth to 433.4 cGy.min^{-1} and reduced the treatment time to less than 1 min. However, this substantial improvement in treatment efficiency was accompanied by poor dose uniformity in both the depth and lateral directions. The region encompassed by the 100% isodose was narrow, and a tumor with a diameter of 2.0 cm was covered only by an isodose level of approximately 30%. This dose-distribution pattern indicates a substantial risk of target underdosage. Therefore, although the plaque geometry offers a major practical advantage in terms of treatment time, its dosimetric characteristics were not clinically acceptable under the investigated configuration.

On balance, these findings indicate that, under the treatment conditions investigated in the present study, the evaluated beta-emitting source configurations do not provide clinically satisfactory dosimetric performance for intraoral SMB without substantial modification. The treatment scenario was based on a representative clinical approach, including a prescription depth of 0.5 cm and a conventional PMMA mold geometry reported in previous oral BT studies. The primary objective was to assess the feasibility of currently available beta-emitting source designs under these representative conditions rather than to optimize all possible treatment-planning parameters. Although lesion thickness, prescription depth, mold geometry, source activity, and catheter arrangement may influence treatment performance, the limited penetration of beta particles remains a fundamental constraint for targets extending to greater depths.

These findings underscore the need for purpose-designed applicators rather than direct adaptation of existing beta-emitting source geometries. Future development should focus on optimized plaque geometries, patient-specific applicators, distributed or segmented source arrays, alternative source activities and configurations, and potentially hybrid beta-gamma designs. Such innovations may reduce

[DOI: 10.18502/ijpho.v16i4.22759]

treatment time and improve dose conformity and target coverage while preserving the potential advantage of limited dose deposition in surrounding normal tissues. Further studies investigating a broader range of tumor sizes, shapes, locations, prescription depths, and applicator designs are warranted to better define the potential role of beta-emitting sources in intraoral SMB, particularly for pediatric patients where minimizing late toxicity is critical.

Conclusion

This study evaluated the feasibility of using $^{90}Sr/^{90}Y$ and ^{188}Re beta emitting sources for intraoral SMB through MC simulations. Under the treatment conditions investigated in this study, catheter-based configurations produced acceptable dose distributions; however, the limited penetration depth of beta particles resulted in prolonged treatment times at the prescribed depth for a 0.5-cm-thick lesion. The ^{188}Re plaque substantially reduced treatment time but exhibited poor dose uniformity and inadequate lateral target coverage. Therefore, under the investigated lesion characteristics, prescription depth, mold geometry, and source configurations, the evaluated beta-emitting source approaches did not provide clinically satisfactory dosimetric performance for intraoral SMB. These findings highlight the need for further studies to investigate optimized plaque geometries, patient-specific applicators, alternative source configurations and activities, segmented arrays, or hybrid beta-gamma source designs. Such developments may improve target coverage while preserving the intrinsic advantages of beta radiation.

Availability of Data

Available upon reasonable request from the author

Acknowledgements

None. No AI program was used during the development of this research paper.

Conflict of Interest

There is no conflict of interests regarding this research.

Funding

This study did not receive any specific funding from public, commercial, or non-profit agencies.

Ethical Considerations

This study was conducted in accordance with the ethical standards of the Declaration and approved by the Research Ethics Committee of Shahid Sadoughi University of Medical Sciences, Yazd, Iran (Ethics Code: IR.SSU.MEDICINE.REC.1404.083).

Authors' Contributions

Sh.S did the conceptualization and design of the study. MH.Z and Sh.R contributed to the data collection. S.N S and S.H prepared the first draft of the manuscript. Sh.S and Sh.R critically revised and closely checked the proposal, the analysis and interpretation of the data and the design of the article. All the authors read and approved the final manuscript.

Artificial Intelligence Use Disclosure Statement

No artificial intelligence tools were used in this manuscript.

References

1. Ekwelundu E, Krasin MJ, Farr JB. Custom-designed mouthpiece for HDR brachytherapy of embryonal rhabdomyosarcoma of the soft palate. J Contemp Brachytherapy 2014; 6(3):300-303.

2. Jadali F, Goudarzipour K, Aghakhani R, Khoddami M, Arab AM, Behnam B. The frequency of PAX3 and PAX7 Mutations in Children with Rhabdomyosarcoma. Iran J Ped Hematol Oncol 2016; 6(2):105-105.

3. Vennarini S, Colombo F, Mirandola A, Chiaravalli S, Orlandi E, Massimino M, *et al*. Clinical insight on proton therapy for paediatric rhabdomyosarcoma. Cancer Manag Res 2023; 15:1125-1139.

[DOI: 10.18502/ijpho.v16i4.22759]

4. Dávila Fajardo R, Giovanni S, Gaze MN, Boterberg T, Cameron A, Fuchs J, *et al*. Brachytherapy for rhabdomyosarcoma: Survey of international clinical practice and development of guidelines. Radiother Oncol 2024; 195:110273.

5. Corrao G, Mazzola GC, Lombardi N, Marvaso G, Pispero A, Baruzzi E, *et al*. Oral surgery and osteoradionecrosis in patients undergoing head and neck radiation therapy: An update of the current literature. Biomedicines 2023; 11(12):3339-744.

6. Yamazaki H, Yoshida K, Yoshioka Y, Shimizutani K, Furukawa S, Koizumi M, *et al*. High dose rate brachytherapy for oral cancer. J Radiat Res 2013; 54(1):1-17.

7. Rahbar YS, Zare MH, Broomand MA. Estimation of Secondary Cancer Risk of Radiosensitive Organs for Leukemia from Head Radiotherapy in Pediatric Patients. Iran J Ped Hematol Oncol 2023; 13(4):225-232.

8. Mazeron JJ, Ardiet JM, Haie-Méder C, Kovács G, Levendag P, Pieffert D, *et al*. GEC-ESTRO recommendations for brachytherapy for head and neck squamous cell carcinomas. Radiother Oncol 2009; 91(2):150-156.

9. Bahreyni Toossi MT, Abdollahi M, Ghorbani M. A Monte Carlo study on dose distribution validation of GZP6 ^{60}Co stepping source. Rep Pract Oncol Radiother 2012; 18 (2):112-116.

10. Sheikholeslami S, Khodaverdian S, Hashemzaei F, Ghobadi P, Ghorbani M, Farhood B. Evaluation of bone dose arising from skin cancer brachytherapy: A comparison between ^{192}Ir and ^{60}Co sources through Monte Carlo simulations. Comput Methods Programs Biomed 2021; 205:106089.

11. Matsuzaki H, Takemoto M, Hara M, Unetsubo T, Yanagi Y, Katsui K, *et al*. Two-piece customized mold technique for high-dose-rate brachytherapy on cancers of the buccal mucosa and lip. Oral Surg Oral Med Oral Pathol Oral Radiol 2012; 113(1):118-125.

12. Budrukkar A, Dasgupta A, Pandit P, Laskar SG, Murthy V, Upreti RR, *et al*. Clinical outcomes with high-dose-rate surface mould brachytherapy for intra-oral and skin malignancies involving head and neck region. J Contemp Brachytherapy 2017; 9(3):242-250.

13. Mukherji A, Mourougan S, Saravannan K, Vivekanandam S, Reddy KS. Dosimetric analysis and clinical outcomes in CT-based mould brachytherapy in early oral cancers in patients unfit for surgery. J Contemp Brachytherapy 2015; 7(2):147-153.

14. Ma N, Wang P, Zhang S, Ning X, Guo C, Zhang Q, *et al*. Surgical resection and orbital iodine‐125 brachytherapy for orbital malignancy: a novel treatment for orbital lymphoma. Int Ophthalmol 2023; 43(6):1945-1955.

15. Nojima H, Kaida A, Haraguchi M, Murase M, Hattori M, Tomioka H, *et al*. Efficacy of low-dose rate brachytherapy utilizing a mold with gold-198 grains for hard palate and gingival cancer. Oral Radiol 2026; 42(1):197-203.

16. Seraj S, Ghorbani M, Hamzian N, Farhood B. Brachytherapy of skin cancer using a ^{90}Sr/^{90}Y beta-emitting source: design of a fixed geometry applicator. Radiat Oncol 2026; 21(1):95.

17. Finger PT. Yttrium-90 episcleral plaque brachytherapy for choroidal melanoma. J Vitreoretin Dis 2024; 8(2):210-214.

18. Pashazadeh A, Landes R, Boese A, Kreissl MC, Klopfleisch M, Friebe M. Superficial skin cancer therapy with Y-90 microspheres: A feasibility study on patch preparation. Skin Res Technol 2020; 26(1):25-29.

19. Laoues M, Khalifi R, Sidi Moussa A. Comparison between beta radiation dose distribution due to LDR and HDR ocular brachytherapy applicators using GATE Monte Carlo platform. Phys Med 2016; 32(8):1007-1018.

20. Adhikari T, Montenegro T, Jung JW, Oare C, Fonseca G, Beaulieu L, *et al*. The use of Monte Carlo simulation techniques in brachytherapy: A comprehensive literature review. Brachytherapy 2025; 24(4):564-621.

21. Demir B, Ahmed AS, Babalik E, Demir M, Gurmen T. Verification and uniformity control of doses for Sr/Y intravascular brachytherapy sources using radiochromic film

[DOI: 10.18502/ijpho.v16i4.22759]

dosimetry. J Med Phys 2008; 33(2):54-59.

22. International Commission on Radiological Protection. Nuclear Decay Data for Dosimetric Calculations. ICRP Publication 107. Ann ICRP. 2008;38(3).

23. Khorshidi A, Ahmadinejad M, Hosseini SH. Evaluation of a proposed biodegradable ^{188}Re source for brachytherapy application: a review of dosimetric parameters. Medicine 2015; 94(28):e1098.

24. Chiu-Tsao ST, Schaart DR, Soares CG, Nath R. Dose calculation formalisms and consensus dosimetry parameters for intravascular brachytherapy dosimetry: recommendations of the AAPM Therapy Physics Committee Task Group No. 149. Med Phys 2007; 34(11):4126-4157.

25. L Gupta AM, L Pujari, V P Maknikar, A Zaidi, A Kumar. Custom made brachytherapy applicator for squamous cell carcinoma of oral commissures. J Cancer Res Ther 2024; 20(5):1632-5.

26. Seemawati P, Kundu J, Pradhan S, Bhut A, Tiwari K, Vidhyawati P. Mold-based brachytherapy for lip cancer: Case report. IOSR J Dent Med Sci 2025; 24(4):5-7.

27. Salamat F, Siavashpour Z, Sadeghi M, Jaberi R, Gholami S. Dosimetric evaluation and Monte Carlo simulation of a new proposed surface brachytherapy mould. J Contemp Brachytherapy 2024; 16(4):279-288.

28. International Electrotechnical Commission (IEC). Medical electrical equipment-Medical electron accelerators-Functional performance characteristics. IEC 60976 Report 2007.

29. Wang R, Li XA. Dosimetric comparison of two ^{90}Sr/^{90}Y sources for intravascular brachytherapy: An EGSnrc Monte Carlo calculation. Phys Med Biol 2002; 47(23):4259-4269.

30. National Institute of Standards and Technology (NIST), Star database, Composition [Available at: https://physics.nist.gov/cgi-bin/Star/compos.pl?matno=261].

31. Kim CH, Choi C, Bolch WE, Petoussi-Henss N, Zankl M, Lee C, *et al*. ICRP publication 156: paediatric mesh-type reference computational phantoms. Annals of the ICRP 2024; 53((1-2)):11-351.

32. Holmes SM, DeWerd LA, Micka JA. Experimental determination of the radial dose function of ^{90}Sr/^{90}Y IVBT sources. Med Phys 2006; 33(9):3225-3233.

33. DeWerd LA, Ibbott GS, Meigooni AS, Mitch MG, Rivard MJ, Stump KE, et al. A dosimetric uncertainty analysis for photon-emitting brachytherapy sources: report of AAPM Task Group No. 138 and GEC-ESTRO. Med phys 2011; 38(2):782-801.

34. Budrukkar A, Dasgupta A, Pandit P, Laskar SG, Murthy V, Upreti RR, *et al*. Clinical outcomes with high-dose-rate surface mould brachytherapy for intra-oral and skin malignancies involving head and neck region. J Contemp Brachytherapy 2017; 9(3):242-250.

35. Reshko LB, Gaskins JT, Bumpous JM, Tennant PA, Khan Z, Sowards K, et al. Surface mould brachytherapy in oral and oropharyngeal cancers. Contemp Oncol (Pozn) 2021; 25(4):254-263.

36. Takácsi-Nagy Z, Ferenczi O, Major T, Akiyama H, Fröhlich G, Oberna F, *et al*. Results of sole postoperative interstitial, high-dose-rate brachytherapy of T1-2 tongue tumours. Strahlenther Onkol 2022; 198(9):812-819.

37. Bhalavat R, Budrukkar A, Laskar SG, Sharma D, Mukherji A, Chandra M, *et al*. Brachytherapy in head and neck malignancies: Indian Brachytherapy Society (IBS) recommendations and guidelines. J Contemp Brachytherapy 2020; 12(5):501-511.

38. Ferreira C, Johnson D, Rasmussen K, Leinweber C, Ahmad S, Jung JW. A novel conformal superficial high-dose-rate brachytherapy device for the treatment of nonmelanoma skin cancer and keloids. Brachytherapy 2017; 16(1):215-222.

39. Pashazadeh A, Castro NJ, Morganti E, Lagotzki S, Boese A, Hutmacher DW, *et al*. Conceptual design of a personalized radiation therapy patch for skin cancer. Curr Dir Biomed Eng 2018; 4(1):607-610.

40. Sedda AF, Rossi G, Cipriani C, Carrozzo AM, Donati P. Dermatological high-dose-rate brachytherapy for the treatment of basal and squamous cell carcinoma. Clin Exp Dermatol

[DOI: 10.18502/ijpho.v16i4.22759]

2008; 33(6):745-749.

41. Castellucci P, Savoia F, Farina A, Lima GM, Patrizi A, Baraldi C, et al. High dose brachytherapy with non sealed ^{188}Re (rhenium) resin in patients with non-melanoma skin cancers (NMSCs): single center preliminary results. Eur J Nucl Med Mol Imaging 2021; 48(5):1511-1521.

42. The American Brachytherapy Society - Ophthalmic Oncology Task Force. The American Brachytherapy Society consensus guidelines for plaque brachytherapy of uveal melanoma and retinoblastoma. Brachytherapy 2014; 13(1):1-14.

[DOI: 10.18502/ijpho.v16i4.22759]